JOURNAL OF MATERIALS SCIENCE **38** (2003) 2393–2399

Cavitation asymmetry in silicon nitride by scanning laser acoustic microscopy

F. LOFAJ
Institute für Keramik im Maschinenbau, Universität Karlsruhe, 76131 Karlsruhe, Germany
E-mail: lofaj@saske.sk

V. LUPRANO
Centro Nazionale per La Ricerca e Lo Sviluppo dei Materiali (CNRSM), 721 00 Brindisi, Italy

Scanning laser acoustic microscopy (SLAM) was used to visualize creep damage distribution in the gas-pressure-sintered silicon nitride after creep at 1300°C in 4-point bending. SLAM revealed asymmetrical distribution of creep damage beneath the tensile surface and in a narrow zone that spread continuously across the neutral axis toward the compression surface. Scanning and transmission electron microscopy confirmed the presence of cavities in tensile zone of bending bar. The combination of the homogeneous cavity development in the zone of tensile stresses and formation of the damage zone ahead of main crack was proposed to explain such cavity distribution. Current SLAM observation is a direct evidence of cavitation asymmetry in vitreous bonded ceramics. Such distribution supports the model of simultaneous presence of cavitation and non-cavitation creep mechanisms in silicon nitride and similar ceramics.

1. Introduction

More than 20 year of intensive research and development in silicon nitride ceramics resulted in significant progress in technology and improvement in its mechanical properties [1–3]. Despite that, economical reasons and the problems with the behavior at elevated temperatures in aggressive environment prevent wider commercial application of these ceramics. Creep is among the principal limitations for long-term use at high temperatures under stress, e.g., for blades in the ceramic gas turbines. At least two principal problems were identified over the years in creep of structural ceramics: disagreement between theoretical models and high sensitivity to stress [3] and asymmetry in creep behavior in tension and compression [4–9].

The attempts to explain high stress exponents and creep asymmetry are commonly related to different extent of cavitation [7, 10, 11]. According to the simplest models [4, 12, 13], cavitation tensile strain can be produced when the adjacent grains separate faster than the accommodation of grain movement due to the viscous flow of the amorphous boundary phase. Each cavity is directly transformed into an increment of tensile strain and increases strain rate [14], which results in creep asymmetry [6, 7].

Recent model of Luecke and Wiederhorn [15] considers cavitation as the main tensile creep mechanism and predicts exponential dependence on stress. After loading, grain boundary sliding (GBS) results in the formation of dilatation tensile stresses at multigrain junctions. Some of the stresses exceed threshold stress for nucleation and cavities develop in those junctions. They subsequently grow via redistribution of the secondary phases by solution-precipitation among junctions with different levels of dilatation stresses. Exponential dependence on stress explains the existence of a wide range of the measured stress exponents. However, the comparison of tensile and compressive rates revealed that both rates converge and creep asymmetry practically disappears at low stresses [6]. Stress exponent approaches unity, cavitation and non-cavitation creep at these conditions became indistinguishable. Simple theoretical analysis showed that all volume of cavities contributes to tensile strain [7], not only one third of the volume as it was assumed earlier [16]. Additional density measurements, ultrasonic wave velocity measurements and other methods revealed that cavities produce more than 70% of total tensile strain [1, 7, 14, 17–20]. Thus, cavitation is the main creep mechanism in some silicon nitride ceramics.

Bending is experimentally very simple method for simultaneous investigation of both tensile and compressive deformation in the same sample. The differences in strain rates and cavitation are so significant that they leads to the time dependent stress redistribution within the bending bar and a shift of the neutral axis toward compression surface [8, 9, 21]. Because of stress redistribution, time dependent and nonsymmetrical creep cavitationdamage development can be expected [6, 7, 9, 21, 22]. The visualization of the cavity distribution in bending specimen would be useful for approving or disapproving the ideas involved in cavitation creep models and to contribute to the understanding of the relationship between various deformation mechanisms. The aim of this paper is to visualize bending creep damage distribution in gas-pressure-sintered silicon nitride

at the late stage of deformation using scanning laser acoustic microscopy to contribute to better understanding of the role of cavitation in creep asymmetry.

2. Experimental procedure

2.1. Material preparation

Material studied was prepared from commercial silicon nitride powder LC 12 SX (H.C. Starck) and additives of 9 wt% of Y_2O_3 and 1 wt% of Al_2O_3 (H.C. Starck) at IKTS (Fraunhofer—Einrichtung für keramische Technologien und Sinterwerkstoffe, Dresden, Germany). The starting powder and additives were mixed and homogenized 4 hrs in isopropanol. The 5 mm × 6 mm × 60 mm bars were formed by cold pressing at 200 MPa and sintered at 1900°C and pressure of 50 bars for 90 min. The microstructure consisted from elongated ß-Si_3N_4 grains with the diameter in the range 0.5–1 μm and aspect ratio higher than 5. Secondary phases were partially crystallized as yttrium disilicate and residual glass always separated them from the silicon nitride grains. Bending specimens with the dimensions 3 mm × 3 mm × 45 mm were cut from the sintered bars and their surfaces were ground by diamond wheels. The tensile surface of the specimens was polished up to 1 μm finish and their edges chamfered.

2.2. Bending creep testing

Four point bending tests were carried out in argon in bending creep test furnace (HTTF 1A, SFL—Instron, Inc., UK) with lever arm and dead weight loading. Neutral atmosphere was used to prevent oxidation effects, which could interfere with the subsequent acoustic measurements. The outer/inner spans between rollers were 40 mm and 20 mm, respectively. Samples were heated with the rate of 3°C/min up to predetermined temperature and 1 hr dwell prior to loading was used for temperature stabilization. The results of earlier 4-point-bending creep study on this material [23] were used for the determination of the creep conditions for the study of cavitation. Testing temperature of 1300°C and initial outer fiber stress 65 MPa in flowing argon were chosen. The lifetime of the material at these conditions was approximately 10–12 hrs, which was suitable for intermittent creep experiments.

The creep test was interrupted and the same specimen was cooled down under load after 0.75 hr and then after 8.5 hrs of deformation. They corresponded to approximately 7.5% and 85% of the lifetime, respectively and strains of ∼0.3% and 1.3%.

2.3. Scanning laser acoustic microscopy

The initial state of the specimen and the state after each interrupted creep test were investigated by scanning laser acoustic microscope (Sonoscope 2140, Sonoscan Inc., Bensenville, Chicago, USA) at CNRSM. The scanning laser acoustic microscope (SLAM) used continuous plane ultrasonic waves with the frequency of 100 MHz in transmission mode to detect the changes of the microstructure or the defects in the sample. A scanning laser beam was used as an ultrasonic detector [24]. The distribution of the defects was determined from the relative gray level of pixels after the digitalization of the SLAM image. The darker zones corresponded to higher attenuation of ultrasonic waves on the defects in the microstructure and the difference in gray level of pixels between the zones subjected to tensile and compressive stresses indirectly indicated their size and/or relative concentration.

SLAM technique is unable to visualize individual defects in the microstructure due to their overlapping in transmission mode and relatively low resolution of the technique. The defects were identified by scanning (SEM) and transmission electron microscopy (TEM). The unfailed specimens were broken after SLAM at room temperature and the secondary fracture surfaces were observed by SEM. The microstructure of the deformed zones in the vicinity of the tensile surface and from the zone outside the outer rollers for comparison were studied by transmission electron microscopy (model 2010, JEOL, Japan) on thin foils prepared by hand grinding, polishing, dimpling and ion milling.

3. Results

3.1. SLAM observation

Fig. 1A shows SLAM image of the as-received material from the central zone of the bending bar. The tensile surface is at the bottom of the image. The material exhibited relatively homogeneous distribution of ultrasonic attenuation over the whole sample, which confirms homogeneity of the material. Fig. 1B is the image of the same area after short time (0.75 hr) creep deformation. Obviously, material is less homogeneous and small changes are clearly visible beneath the tensile surface. Finally, Fig. 1C indicates considerable differences in the ultrasonic attenuation after 8.5 hrs exposure in the zone of tensile stresses while the part of specimen subjected to compression stresses revealed homogeneous attenuation except relatively narrow central area. After digitization of the images, the differences in different areas of the bending bar can be estimated from the histograms of the gray level of the pixels with the same intensity. Fig. 2A and B illustrate the distributions of the gray level of pixels in the zone of tensile and compressive stresses, respectively. The main difference between distributions is in the number of pixels of the same intensity in different zones. These differences in the intensity were quantified over the whole bending bar as it is schematically shown in Fig. 3. Two principally different areas were obtained: (1) the zone subjected to tensile stresses with high ultrasonic attenuation, which corresponds to high concentration and/or large size of creep damage, and (2) the zone with compressive or zero stresses with low attenuation and low concentration of creep damage. Frame 3 determines the area of the specimen shown in the acoustical micrograph in Fig. 1C. Note an irregularity in damage distribution in the center of the sample, which is symmetrically extended from tensile zone into compressive zone.

3.2. SEM observation

The tensile and compression surfaces of the specimen after final SLAM observation were polished to remove

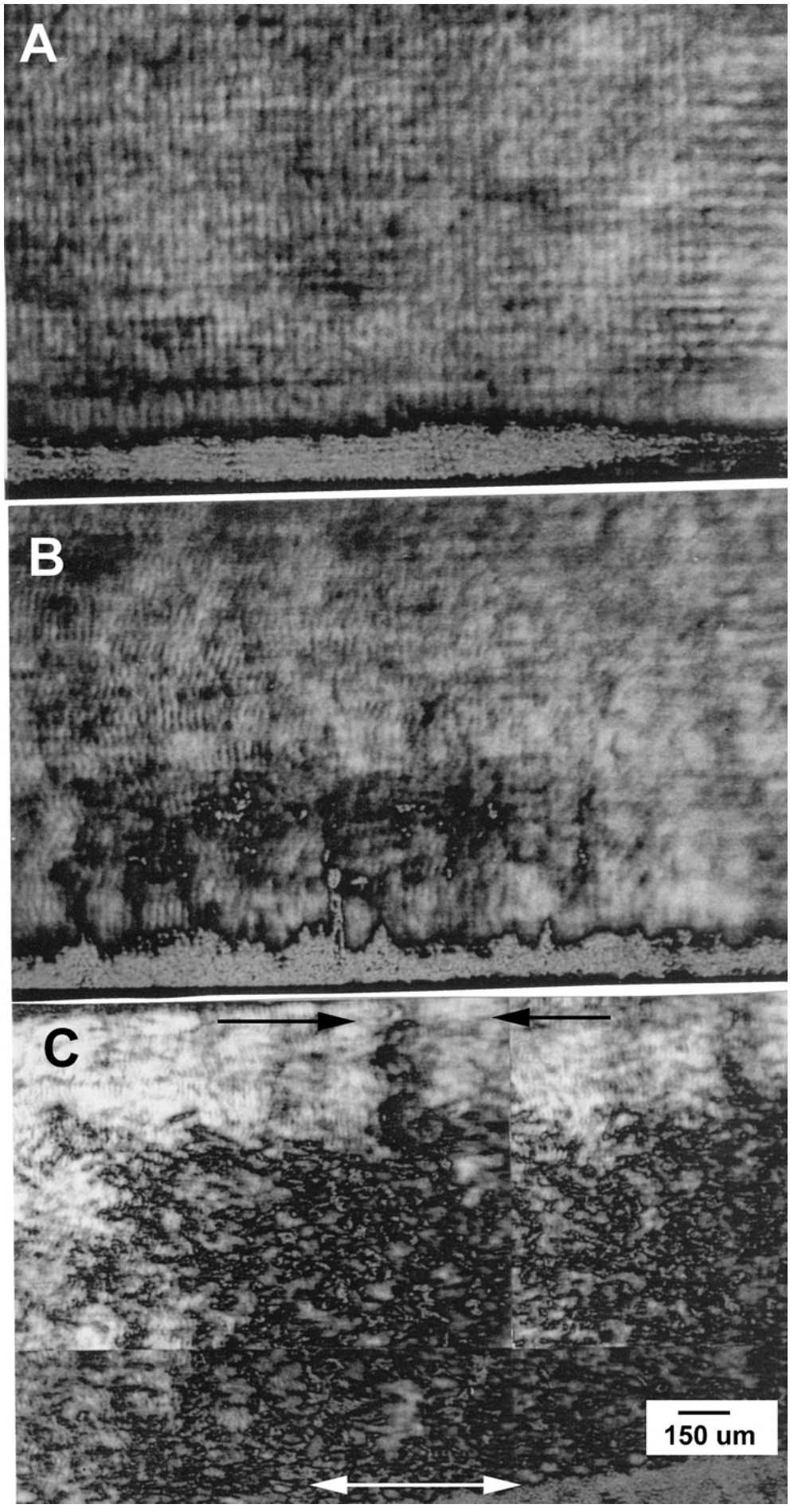

Figure 1 SLAM micrographs of the GPS silicon nitride in the as-received state—(A), after the first creep deformation at 1300°C under stress of 65 MPa for 0.75 hrs—(B), and after creep at the same conditions for 8.5 hrs—(C). The darker zone below the tensile surface corresponds to higher ultrasonic attenuation due to the presence of creep damage.

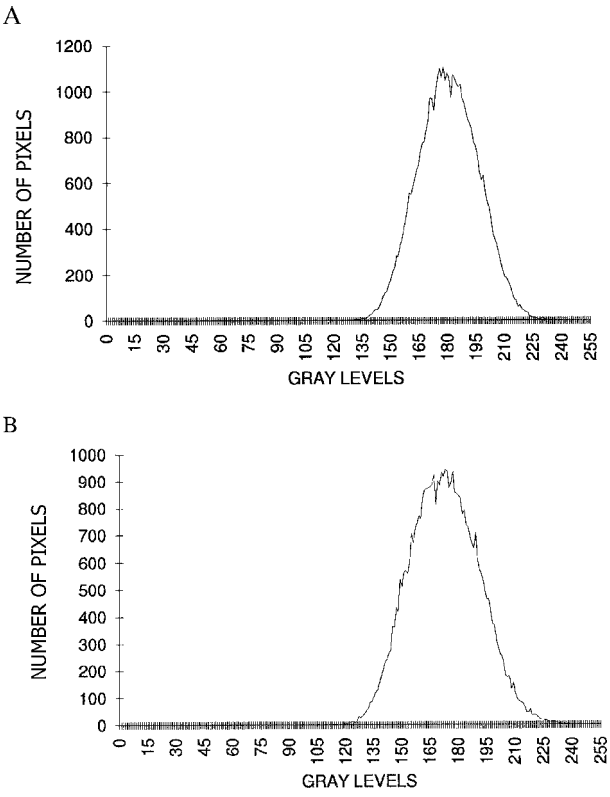

Figure 2 Histograms of the gray levels of the pixels from digitized image shown in Fig. 1C in the zone of tensile stresses—(A) and compressive stresses—(B). The differences in number of pixels with the same gray level results from higher attenuation in the damaged zone.

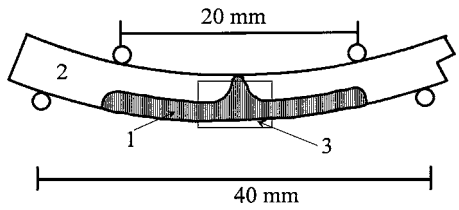

Figure 3 Schematic distribution of creep damage in the bending bar after creep 1300°C/65 MPa/8.5 hrs. Two zones are indicated: (1) zone with high concentration of creep damage, and (2) zone with low concentration of creep damage. The frame (3) corresponds to the area shown on Fig. 1C. The missing part of specimen was used for the preparation of thin foil from undeformed material.

surface layers. Fig. 4A and B are SEM micrographs of the microstructure after creep from the zones beneath compressive and tensile surfaces, respectively. Numerous voids with bimodal size distribution were present in the microstructure. Larger voids with the size of >3 μm correspond to pores, which are relatively homogeneously distributed in the material volume. Small voids with the size below $\sim$0.5 μm seem to be cavities since they are mostly present in the area subjected to tensile stresses. Large cracks were not observed.

The microstructure in the zones close to compressive surface, neutral axis and tensile surface taken from secondary fracture surfaces are illustrated in Fig. 5A–C, respectively. The grains in the zone of compressive stresses are close to each other (Fig. 5A) whereas grains are separated if subjected to tensile stresses (Fig. 5C). The microstructure around neutral axis showed few cavity-like intergranular pockets (see arrow in Fig. 5B). Relatively many empty intergranular areas visible in each zone seem to result from the character of the secondary fracture surfaces.

3.3. TEM study

The observation of the microstructure of the crept specimen from the zone of tensile stresses agreed with SEM observations. Relatively many creep cavities were found in the glassy phase both at multigrain junctions (Fig. 6A) and two-grain junctions (Fig. 6B). The size of multigrain junction cavities was comparable with the grain size, while the size of oblate cavities on grain facets was considerably smaller. The different size of both kinds of cavities indicated different time of their nucleation and/or very different growth rate. Besides cavities, TEM revealed the presence of strain whorls [25].

4. Discussion

SLAM and SEM/TEM observations of microstructure changes after creep deformation revealed the presence of creep damage, initial porosity and cavitation, respectively. Although electron microscopy techniques are unable to determine the quantitative differences in the concentration of the cavities in different zones and SLAM yields only the integrated image of creep defects, the combination of both methods and numerous earlier observations suggest that SLAM visualizes distribution of creep cavities and/or their relative concentration. The effect of the initial porosity is eliminated due to comparison of different zones and provided porosity is homogeneously distributed.

Cavitation occurs predominantly in the amorphous phase when critical local stress level is reached. Multigrain junctions and ledges on grain facets in combination with grain boundary sliding act as the local stress concentrators for cavity nucleation [4, 10, 11, 26, 27]. Therefore, the distribution revealed by SLAM should be related to the distribution of critical local tensile stresses for cavity nucleation. However, since the nuclei size is considerably smaller than the detection limit of the acoustic microscopy, Fig. 3 relates to the distribution of large cavities.

According to Fig. 3, creep cavities developed asymmetrically with regard to neutral axis. The zone of tensile stresses was much more cavitated than the zone of compressive stresses. Thus, besides asymmetry in creep rates well known in ceramics, SLAM provides direct evidence for asymmetry of creep cavitation. It is noteworthy that the zone with high content of creep damage beneath tensile surface was smaller than the distance to the neutral axis. All these conclusions can be understood based on earlier models of creep cavitation and recent cavitation model of Luecke and Wiederhorn [15]. Obviously, cavity nucleation requires reaching critical level of tensile stresses. Number of junctions with critical stresses is the highest in the zone of maximum stresses and gradually decreases toward neutral axis. Because of stress distribution across the bending bar, local stresses at certain distance from neutral axis

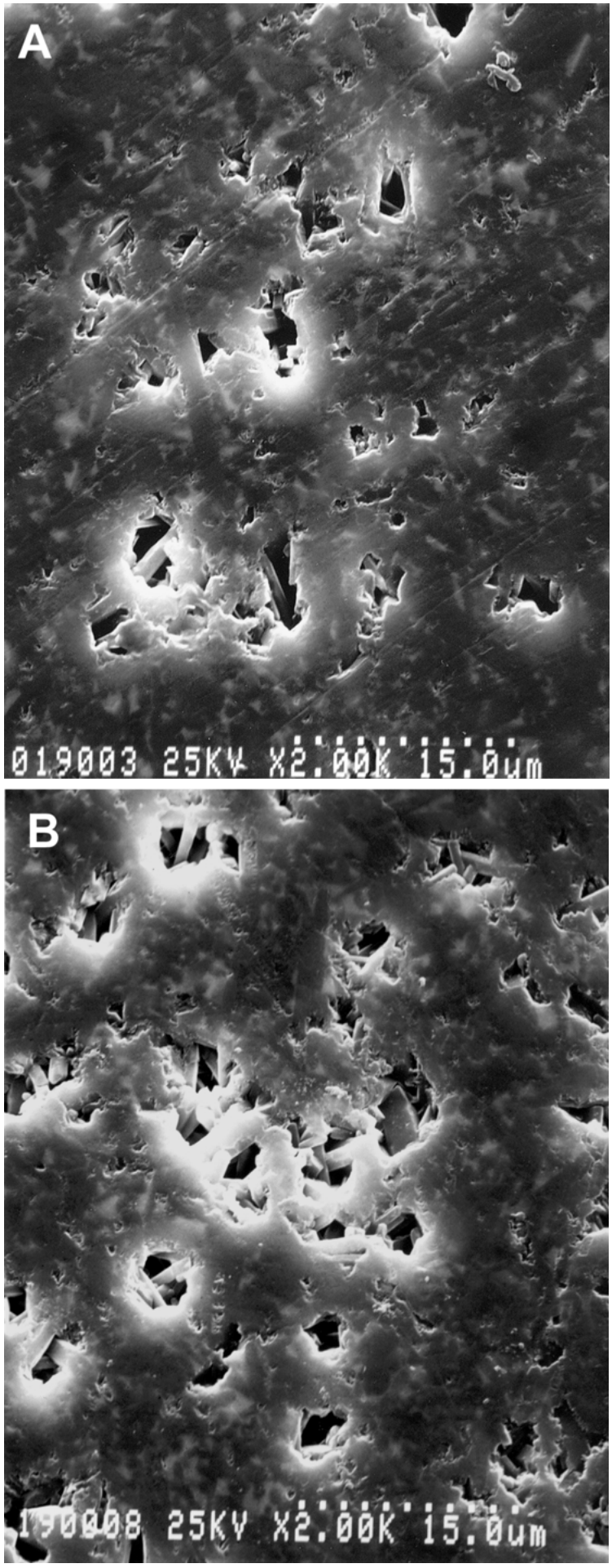

Figure 4 SEM micrographs from the polished surfaces subjected to compressive stresses—(A) and tensile stresses—(B). Large pores are present on both surfaces but additional small cavity-like pores are present on tensile surface.

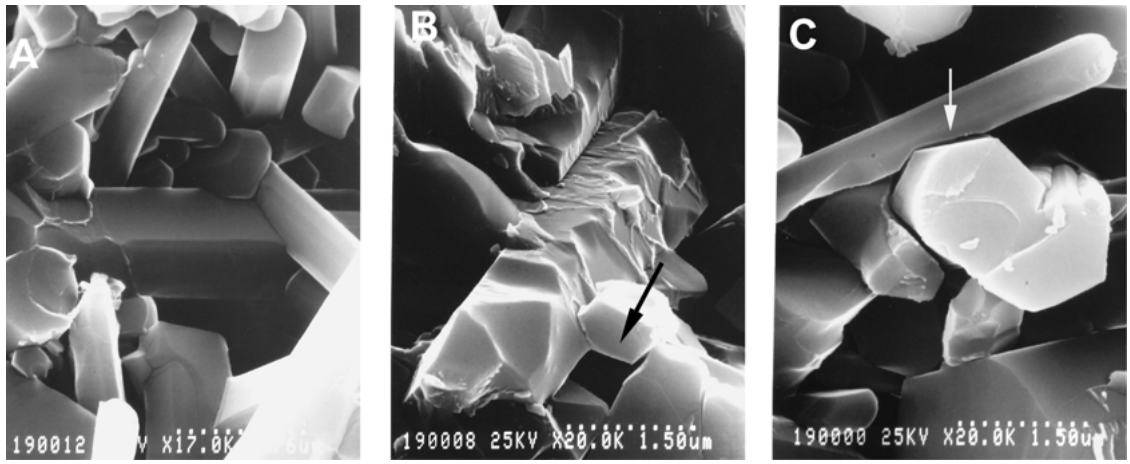

Figure 5 SEM micrographs from the secondary fracture surface in the zone of compressive stresses—(A), near neutral axis—(B), and near the surface subjected to tensile stresses—(C). The arrows in Fig. 5B and C indicate multigrain junction cavity and grain separation, respectively.

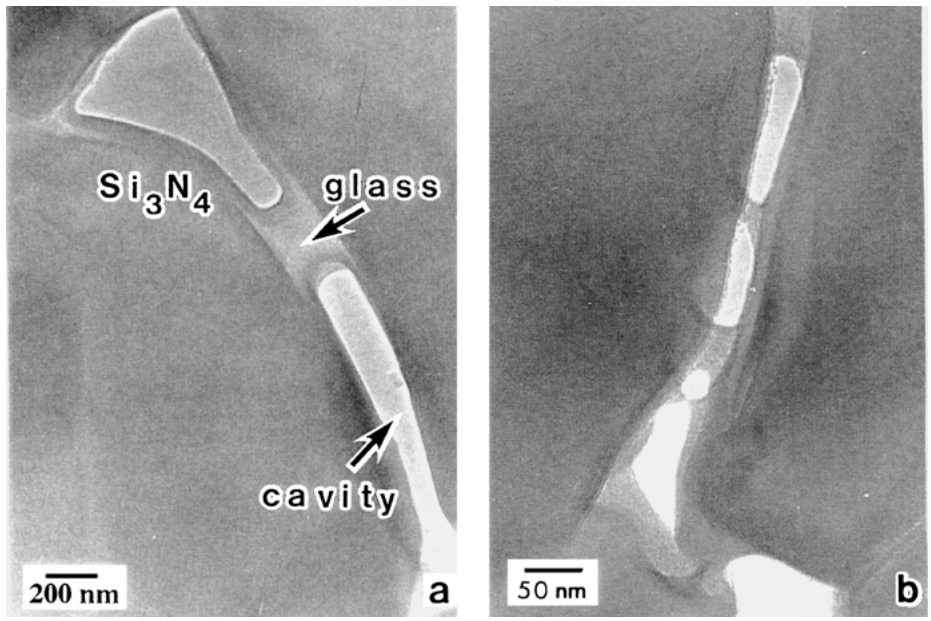

Figure 6 The details of creep cavities: (a) mutual growth of two cavities in glassy phase from triple points and (b) multiple cavities at two-grain junction.

are insufficient and cavitation becomes impossible. Thus, damaged zone is thinner and the transition zone between highly cavitated and "uncavitated" area is very narrow. However, the presence of some cavities in the zone of compression cannot be excluded since GBS results in development of dilatational hydrostatic tensile stresses even at the multigrain pockets among grains subjected to compression. Asymmetrical cavity distribution indicates also a difference in the conditions for subsequent cavity growth and further evolution throughout the bending bar.

Contrary to the above theoretical considerations is the fact that the zone with high concentration of creep damage spread through the neutral axis zone into the zone of compressive stresses in the narrow central part of the bending bar (see Fig. 3). The width of this zone is considerably smaller than the inner rollers span. Damage theory [28] assumes crack formation only under tensile stresses. The reason may be connected with the existence of large crack, which locally increased the stress level and enhanced cavitation as shown in Fig. 7. At the early stages of creep deformation, cavities formed homogeneously in the zone beneath tensile surface. Considerably higher cavity growth rate in the region of tensile stresses in comparison with the zone of compressive stresses led to enhanced cavitation beneath the tensile surface in between inner rollers. At the later stage of deformation, coalescence of cavities would result in the formation of a main crack [27]. The case becomes similar to the notched or pre-cracked specimen, when the crack velocity toward compression surface is controlled by the stress intensity factor regardless of the cavity concentration in the surrounding matrix [9]. The elastic fields at the crack tip change the level of constraints and promote its slow propagation toward compression surface. The driving force is restricted to the small region of the "process zone" at the crack tip. Slow crack growth occurs until critical size is reached and specimen fails catastrophically. Thus, while creep damage during deformation is the result of continuous development of cavities in the zone with sufficiently high tensile stresses, creep rupture results from the slow

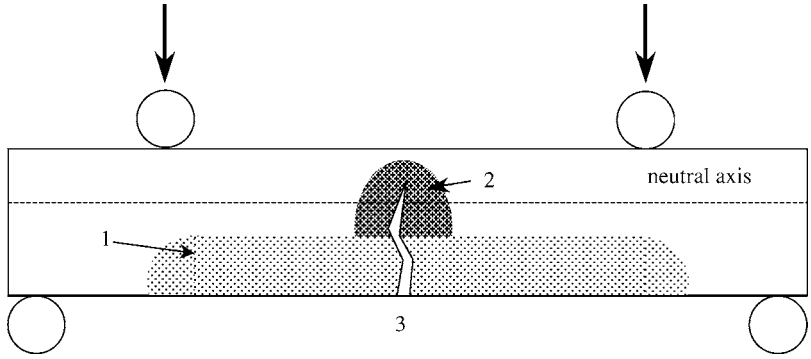

Figure 7 Schematic illustration of bending creep damage development at the late stage of deformation: homogeneous creep cavitation in the zone of tensile stresses (1) and creep damage zone (2) ahead of the main crack (3).

crack growth limited to the damage zone at the main crack tip.

5. Conclusions

SLAM observation of the gas pressure sintered silicon nitride crept in 4-point bending visualized damage distribution in the bending specimen at the late stage of deformation. Subsequent SEM/TEM studies showed that this damage corresponds to the increase in cavity concentration. Large number of creep cavities was observed beneath the tensile surface in between inner rollers and in a narrow zone that spread continuously across the neutral axis toward compression surface, whereas considerably less of cavities developed in other zones. The differences in cavity development were assumed to result from the stress distribution within the bending bar. The combination of the homogeneous cavity development in the zone of tensile stresses and formation of the damage zone ahead of main crack was proposed to explain the extension of creep damage into a narrow zone of compressive stresses. Current SLAM observation can be considered as direct evidence of cavitation asymmetry, which results in asymmetry in creep resistance in vitreous bonded ceramics. Such distribution supports the model of simultaneous presence of cavitation and non-cavitation creep mechanisms in silicon nitride and similar ceramics.

Acknowledgment

The authors are very grateful to H. Klemm and M. Herrmann (IKTS, Dresden, Germany) for the supply of specimens and to M. Reece (QMW College, University of London) and P. Hvizdoš (IMR SAS) for the assistance with TEM study. The work was partially supported by Alexander von Humboldt Foundation and VEGA Grant No. 2/7011/20.

References

1. S. M. WIEDERHORN, *Z. Metallkd.* **90**(12) (1999) 1053.
2. F. LOFAJ, S. M. WIEDERHORN, G. G. LONG, P. R. JEMIAN and M. K. FERBER, in "Ceramic Materials and Components for Engines," edited by J. G. Heinrich and F. Aldinger (DKG and Wiley-VCH, Weinheim, Germany, 2001) p. 487.
3. F. LOFAJ, S. M. WIEDERHORN, G. G. LONG, B. J. HOCKEY, P. R. JEMIAN, L. BROWDER, J. ANDREASON and U. TÄFFNER, *J. Eur. Ceram. Soc.* **22** (2002) 2479.
4. F. F. LANGE, in "Deformation of Ceramic Materials," edited by R. C. Bradt and R. E. Tressler (Plenum Press, New York, 1975) p. 361.
5. M. K. FERBER, M. G. JENKINS and V. J. TENNERY, *Ceram. Eng. Sci. Proc.* **11** (1990) 1028.
6. K. J. YOON, S. M. WIEDERHORN and W. E. LUECKE, *J. Amer. Ceram. Soc.* **83**(8) (2000) 2017.
7. F. LOFAJ, A. OKADA and H. KAWAMOTO, *ibid.* **80**(6) (1997) 1619.
8. T. FETT, K. KELLER and D. MUNZ, *J. Mater. Sci.* **23** (1988) 467.
9. C. F. CHEN and T. J. CHUANG, *J. Amer. Ceram. Soc.* **73**(8) (1990) 2366.
10. A. G. EVANS and A. RANA, *Acta Metall.* **28**(2) (1980) 129.
11. J. E. MARION, A. G. EVANS, M. D. DRORY and D. R. CLARKE, *ibid.* **31**(10) (1983) 1445.
12. J. R. DRYDEN, D. KUCEROVSKY, D. S. WILKINSON and D. F. WATT, *ibid.* **37**(7) (1989) 2007.
13. M. M. CHADWICK, D. S. WILKINSON and J. R. DRYDEN, *J. Amer. Ceram. Soc.* **75**(9) (1992) 2327.
14. W. E. LUECKE, S. M. WIEDERHORN, B. J. HOCKEY, R. E. KRAUSE JR. and G. G. LONG, *ibid.* **78**(8) (1995) 2085.
15. W. E. LUECKE and S. M. WIEDERHORN, *ibid.* **82**(10) (1999) 2769.
16. C. J. GASDASKA, *ibid.* **77**(8) (1994) 2408.
17. A. OKADA and F. LOFAJ, *J. Eur. Ceram. Soc.* **20**(10) (2000) 1521.
18. J.-W. CAO, F. LOFAJ and A. OKADA, *J. Mater. Sci.* **36** (2001) 1301.
19. F. LOFAJ, D. T. SMITH, G. V. BLESSING, W. E. LUECKE and S. M. WIEDERHORN, *ibid.*, to be published.
20. F. LOFAJ, *Metallic Materials* **40**(3) (2002) 184.
21. C. F. CHEN, S. M. WIEDERHORN and T. J. CHUANG, *J. Amer. Ceram. Soc.* **74**(7) (1991) 1658.
22. T. J. CHUANG and S. M. WIEDERHORN, *ibid.* **71**(7) (1988) 595.
23. F. LOFAJ, J. DUSZA, M. HERRMANN and H. KLEMM, *Ceramic Forum International—Forschrittberichte der DKG* **9**(4) (1994) 29.
24. L. W. KESSLER, in Proceedings of IEEE, Vol. 67, No. 4, 1978, p. 526.
25. S. M. WIEDERHORN, B. J. HOCKEY, D. C. CRANMER and B. YECKLEY, *J. Mater. Sci.* **28** (1993) 445.
26. M. D. THOULESS, C. H. HSUEH and A. G. EVANS, *Acta Metall.* **31**(10) (1983) 1675.
27. K. S. CHAN and R. A. PAGE, **76**(4) (1993) 803.
28. A. R. ROSENFIELD, W. H. DUCKWORTH and D. K. SHETTY, *J. Amer. Ceram. Soc.* **68**(9) (1985) 483.

Received 28 June 2002
and accepted 21 January 2003